ISSN 1330-3651
UDC/UDK 621.873.15:531.395

A SLEWING CRANE PAYLOAD DYNAMICS

Ivica Marinović, Denijal Sprečić, Boris Jerman

Original scientific paper

To enable an optimum crane design concerning static and fatigue analyses and to enable development of an optimal crane control algorithms the dynamics of the crane and the suspended payload must be well identified. The paper presents a multi-mass model of a slewing crane designed for consideration of slewing motion of the crane that produces the spatial oscillation of the payload. To ensure sufficient accuracy the presented model consists of six masses and account for the non-linear nature of the swinging motion and the non-linearity of the power transmission. The elasticity and damping of the load-bearing steel structure as well as the friction in the main bearing, and the air resistance are also considered. The angles of the payload sway and the dynamic forces are obtained. For the purpose of the confirmation of the mathematical model a comparison of the simulated and measured results was prepared and good agreement was estimated.

Keywords: *cranes, dynamic loading, equations of motion, non-linear dynamic systems, payload sway, slewing motion*

Dinamika korisne nosivosti okretljive dizalice

Izvorni znanstveni članak

Kako bi se omogućila optimalna konstrukcija dizalice u odnosu na statičke analize i analize zamora te kako bi se omogućio razvoj optimalnog algoritama upravljanja dizalice, mora biti dobro identificirana dinamika dizalice i ovješeni korisni teret. Članak prikazuje višemaseni model okretne dizalice konstruirane za razmatranje okretnog gibanja dizalice koja proizvodi prostorno titranje korisnog tereta. Kako bi se osigurala dovoljna točnost predstavljeni model se sastoji od šest masa i procjene za nelinearnu narav okretnog gibanja i nelinearnosti prijenosa snage. U obzir su također uzeti elastičnost i prigušenje nosive čelične konstrukcije, kao i trenje u glavnom ležaju, te otpor zraka. Dobiveni su kutovi njihanja korisnog tereta i dinamičke sile. Radi potvrde matematičkog modela pripremljena je usporedba simuliranih i mjerenih rezultata i procijenjena je dobra podudarnost.

Ključne riječi: *dizalice, dinamičko opterećenje, jednadžbe gibanja, nelinearni dinamički sustavi, njihanje korisnog tereta, okretno gibanje*

1 Introduction

A study of slewing cranes and possible improvements to their performance is a study with a real-life application, because these types of cranes are widely used in ports, on big ships and in civil engineering [1]. The operation of slewing cranes involves three main motions: the slewing motion of the jib around the vertical axis, the radial movement of the load suspension point (trolley movement or the luffing of the jib) and the hoisting of the load (lifting or lowering). In this paper, the slewing motion of a crane, during which the spatial motion of the suspended load is introduced, was looked at in more detail. The same motion was also investigated using a previously developed mathematical model [2].

The dynamic loads caused by the crane's (or trolley's) accelerations and decelerations represent an important part of the loadings of the crane's steel structure [3]. Time depending loads can also be imparted by the crane's skewing [4], the crane's travelling on uneven surfaces, by centripetal accelerations, etc. However, the swinging of the payload is the most important contributor to crane's dynamic loads. Once these loads are known, it is then possible to predict a load spectrum that is the basis for modern fatigue and reliability design. To estimate the fatigue life of the structure and to determine the stress intensity factor, further investigations are necessary. For that a variety of methods can be used, such as approximate analytical methods, finite element method, finite element alternating, weight function, photo elasticity and fatigue tests [5].

The majority of published papers and conference contributions on payload dynamics deal with control strategies and techniques for load-swing suppression. The mathematical models introduced for this purpose can be simplified to a great extent. A couple of examples of such models can be found in [6 ÷ 9]. For other models, see [3].

In contrast, studies of the dynamics of the payload and the influence of payload swinging on the loading of the crane's steel structure have not been investigated to the same extent. These studies can be divided into those that consider the curved motion of the suspension point (typical for slewing cranes performing a slewing motion and also for rubber-tyred gantry cranes changing their direction of motion (turning)) [10 ÷ 12] and those that consider the linear motion of the load suspension point (typical for gantry and overhead-travelling cranes) [13 ÷ 19, 26]. A specific model of moving oscillator, which presents cranes with resilient trolley suspension system is given in [20]. The dynamics of the elevators is investigated in [21].

The majority of the mathematical models used to describe the considered crane structures are simplified by the introduction of all or many of the following assumptions: small angles of the payload sway, a non-deformable structure for the crane, a non-extensible load-carrying rope, and dissipative and other non-linear effects that are neglected for reasons of simplicity.

In order to determine the dynamic loads, models that are more complex must be used. Recent reports suggest the use of more complex models for control purposes too [3]. Complex models can also be used for determination of response of the structure subject to the earthquake excitation, where in the case of more rigid structures larger loadings are expected [22]. For these reasons, an enhanced version of a mathematical model of a general-type slewing crane was developed, based on authors experiences [2, 23, 24], taking into account most of the

frequently neglected features.

2
The multi-mass model of a slewing crane
2.1
Description of the model

The proposed non-linear mathematical model of a slewing crane during the slewing motion is shown in Fig. 1. The model takes into account the elasticity and the material damping in the crane's structure. The air resistance on the payload is also considered, as is the non-linearity of the slewing motion's power transmission, including the friction in the main slewing bearing. The proposed mathematical model accounts for nonlinear nature of the pendulum motion for larger angles of inclination and has therefore no restriction with regard to small angles of the load sway.

The velocity-time profile of the rotating speed $\dot{\varphi}_1$ of a driving shaft is used as an input to the model. This is suitable for the simulation of cases where the speed of the driving motor during acceleration and deceleration is controlled (for instance, by a frequency controller) and for investigating the influence of different profiles of the input angular velocity on the system output.

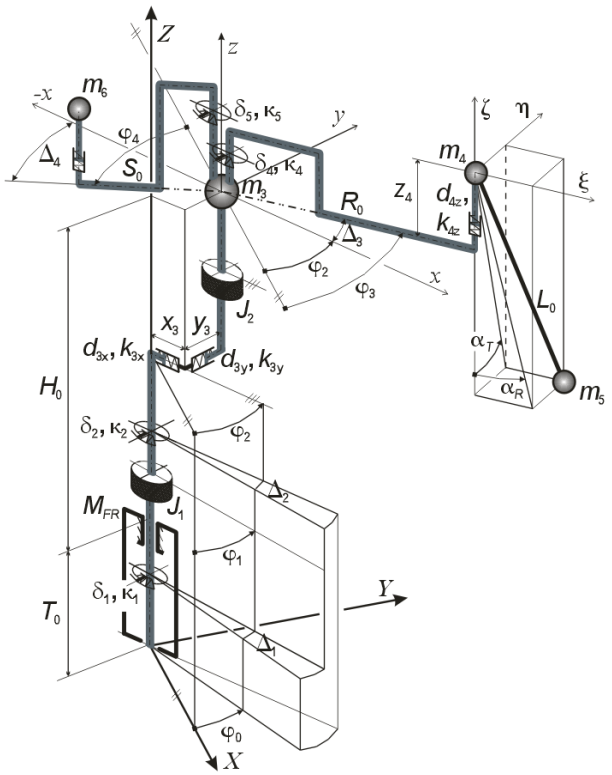

Figure 1 The multi-mass model of a slewing crane

The mass of the crane's structure is represented as follows. The moments of inertia of the rotating platform, and part of the tower (around z-axis), are represented by the moment of inertia J_1. The moments of inertia of the other part of the tower, the part of the counterweight girder, and the part of the jib are represented by the moment of inertia J_2. The mass of the corresponding part of the jib, the mass of the rotating platform and part of the mass of the tower are represented by the point mass m_3. The corresponding part of the mass of the jib and the mass of the trolley (or sheave) are represented by the point mass m_4. The net payload mass and the mass of the load-handling device are represented by the point mass m_5. The mass of the counterweight and the mass of the other part of the counterweight girder are represented by the point mass m_6. The load-carrying rope in the model is represented as mass-less. The influence of its mass on the overall dynamics of the crane is taken into account in the following way. The mass of the upper half of the free length of the payload-carrying rope ($L_0/2$) is added to the mass m_4, and the mass of the lower half is added to the mass m_5.

The elements connecting the masses are weightless. Their stiffness and damping are represented as follows. The properties of the connecting elements between the motor shaft and the rotating platform in terms of torsion (around the z-axis) are represented by the stiffness characteristics κ_1 and the damping characteristics δ_1. Both of them are considered as non-linear. The torsion stiffness of the rotating platform (or tower) around the z-axis is represented by the stiffness coefficient κ_2. Its damping characteristic is represented by the damping coefficient δ_2. The bending stiffness and the damping of the jib around the z-axis are represented by the stiffness coefficient κ_4 and the damping coefficient δ_4. The stiffness and the damping of the rotating platform and of the tower in terms of bending around the y-axis are represented by the stiffness coefficient k_{3x} and the damping coefficient d_{3x}. The stiffness of the jib in terms of the bending around the y-axis is represented by the stiffness coefficient k_{4z} and the damping coefficient d_{4z}. The bending stiffness and the damping of the counterweight girder around the z-axis are represented by the stiffness coefficient κ_5 and the damping coefficient δ_5. The stiffness of the girder in terms of the bending around the y-axis is represented by the stiffness coefficient k_{5z} and the damping coefficient d_{5z}.

The friction in the slewing ring is represented by the moment of friction M_{FR}. The air resistance is represented by the force acting on the point mass m_5, which denotes the influence of the air resistance on the payload.

Three coordinate systems are introduced (Fig. 1). The first is global inertial coordinate system XYZ. The second is the local coordinate system xyz, the x-axis of which rotates together with the rotating platform whereas the z-axis stays parallel to the global Z-axis. The third coordinate system is the local coordinate system $\xi\eta\zeta$, the origin of which is placed at the load suspension point. Its ξ-axis rotates together with the jib whereas the ζ-axis stays parallel to the global Z-axis.

2.2
Formulation of equations of motion

For deriving the differential equations of motion, the second-order Lagrange equations of the following form were used:

$$\frac{\mathrm{d}}{\mathrm{d}t}\left[\frac{\partial T}{\partial \dot{q}_j}\right]-\left[\frac{\partial T}{\partial q_j}\right]+\frac{\partial V}{\partial q_j}=Q'_j \quad j=1,\ldots,10. \tag{1}$$

In Eq. (1) T represents the total kinetic energy of the system and Q_j the non-conservative generalised forces. The influence of the conservative generalised forces is expressed by means of the system's potential energy V. The symbol q_j stands for the independent generalised coordinates: $q_1 = \eta$, $q_2 = \xi$, $q_3 = z_4$, $q_4 = \varphi_3$, $q_5 = y_3$, $q_6 = x_3$, $q_7 = \varphi_2$, $q_8 = \varphi_1$, $q_9 = \varphi_4$, $q_{10} = z_6$.

The next step is to define the speeds of all the mass elements by means of the selected, generalised coordinates. The moments of inertia J_1 and J_2 are rotating with angular speeds $\dot{\varphi}_1$ and $\dot{\varphi}_2$. The speeds of the point masses m_3, m_4, m_5 and m_6 must be represented in the global XYZ frame. The positions of these masses are:

$$X_3 = \cos(\varphi_2)x_3 - \sin(\varphi_2)y_3. \tag{2}$$

$$Y_3 = \sin(\varphi_2)x_3 + \cos(\varphi_2)y_3. \tag{3}$$

$$Z_3 = H_0 + T_0. \tag{4}$$

$$X_4 = \left(\cos(\varphi_3 - \varphi_2)R_0 + x_3\right)\cos(\varphi_2) - \left(\sin(\varphi_3 - \varphi_2)R_0 + y_3\right)\sin(\varphi_2). \tag{5}$$

$$Y_4 = \left(\cos(\varphi_3 - \varphi_2)R_0 + x_3\right)\sin(\varphi_2) + \left(\sin(\varphi_3 - \varphi_2)R_0 + y_3\right)\cos(\varphi_2). \tag{6}$$

$$Z_4 = H_0 + T_0 - \frac{2R_0 x_3}{H_0} + z_4 \tag{7}$$

$$X_5 = -\sin(\varphi_3)\eta - y_3 \cdot \sin(\varphi_2) + \cos(\varphi_3)\cdot(R_0 + \xi) + \cos(\varphi_2)x_3. \tag{8}$$

$$Y_5 = \cos(\varphi_3)\eta + \sin(\varphi_3)\left(R_0 + \xi\right) + \sin(\varphi_2)x_3 + \cos(\varphi_2)y_3. \tag{9}$$

$$Z_5 = H_0 + T_0 + z_4 - \sqrt{L_0^2 - \eta^2 - \xi^2} - \frac{2R_0 x_3}{H_0}. \tag{10}$$

$$X_6 = S_0 \cdot \cos(\varphi_4). \tag{11}$$

$$Y_6 = S_0 \cdot \sin(\varphi_4). \tag{12}$$

$$Z_6 = H_0 + T_0 + \frac{2S_0 x_3}{H_0} + z_6. \tag{13}$$

The associated speeds are the time derivatives of the positions, and the absolute speeds are the vector sums of the components:

$$v_i^2 = \dot{X}_i^2 + \dot{Y}_i^2 + \dot{Z}_i^2 \quad i=3, \ldots, 6. \tag{14}$$

The total kinetic energy T must be expressed by means of generalised coordinates. It is the sum of the individual contributions of all the mass elements:

$$T = \sum_{i=1}^{6} T_i = \sum_{i=1}^{2} \tfrac{1}{2} J_i \dot{\varphi}_i^2 + \sum_{i=3}^{6} \tfrac{1}{2} m_i v_i^2 \quad i=3, \ldots, 6. \tag{15}$$

The potential energy of the system is the sum of the contributions of the potential terms, and is expressed by means of generalised coordinates, as follows:

$$V = \frac{1}{2}k_{3x}x_3^2 + \frac{1}{2}k_{3y}y_3^2 + \frac{1}{2}k_{4z}z_4^2 + \frac{1}{2}\kappa_1(\varphi_1 - \varphi_0)^2 + \frac{1}{2}\kappa_2(\varphi_2 - \varphi_1)^2 + \frac{1}{2}\kappa_4(\varphi_3 - \varphi_2)^2 + \frac{1}{2}\kappa_5(\varphi_4 - \varphi_2)^2 + g\,m_5\left(H_0 + T_0 + z_4 - \sqrt{L_0^2 - \eta^2 - \xi^2} - \frac{2R_0 x_3}{H_0}\right) + g\,m_4\left(H_0 + T_0 + z_4 - \frac{2R_0 x_3}{H_0}\right) + g\,m_6\left(H_0 + T_0 + z_6 - \frac{2S_0 x_3}{H_0}\right). \tag{16}$$

The generalised non-conservative forces (Q_j) are defined through their virtual work δA:

$$\delta A = \delta A_{FR} + \delta A_d + \delta A_{ar}, \tag{17}$$

where the individual components represent the influence of the frictional forces, the damping of the members and the air resistance. The components of virtual work are defined in Eqs. (18) to (20):

$$\delta A_{\mathrm{FR}} = -M_{\mathrm{FR}}\,\delta\varphi_1. \tag{18}$$

$$\delta A_{\mathrm{d}} = -\left(\dot{\varphi}_1 - \dot{\varphi}_0\right)\delta_1\,\delta\Delta_1 - \left(\dot{\varphi}_2 - \dot{\varphi}_1\right)\delta_2\,\delta\Delta_2 - \dot{x}_3\,d_{3x}\,\delta_{x3} - \dot{y}_3\,d_{3y}\,\delta_{y3} - \left(\dot{\varphi}_3 - \dot{\varphi}_2\right)\delta_4\,\delta\Delta_3 - \dot{z}_4\,d_{4z}\,\delta_{z4} - \left(\dot{\varphi}_4 - \dot{\varphi}_2\right)\delta_5\,\delta\Delta_4 - \dot{z}_6\,d_{6z}\,\delta_{z6}. \tag{19}$$

$$\delta A_{ar} = -d_{\mathrm{ar}5}\,v_5\left(\delta X_5\,\dot{X}_5 + \delta Y_5\,\dot{Y}_5 + \delta Z_5\,\dot{Z}_5\right). \tag{20}$$

On the right-hand side of each of Eqs. (18) ÷ (20) there are the terms representing the non-conservative forces (or moments) multiplied by virtual displacements. These equations must be rewritten in terms of the generalised coordinates and the generalised virtual displacements, where appropriate. From the equations arranged in this manner, individual non-zero components of the generalised forces can be obtained as the coefficients near the corresponding virtual displacements. For instance, Eq. (21) is derived from Eq. (18), where the coefficient near the virtual displacement $\delta\varphi_1$ is the negative value of the frictional moment in the slewing ring ($-M_{\mathrm{FR}}$). The same inference leads to Eqs. (22) ÷ (36).

$$Q_{\mathrm{FR}.8} = -M_{\mathrm{FR}}. \tag{21}$$

$$Q_{\mathrm{d}.3} = -d_{4z}\,\dot{z}_4. \tag{22}$$

$$Q_{\mathrm{d}.4} = -\delta_4\left(\dot{\varphi}_3 - \dot{\varphi}_2\right). \tag{23}$$

$$Q_{\mathrm{d}.5} = -d_{3y}\,\dot{y}_3. \tag{24}$$

$$Q_{\mathrm{d}.6} = -d_{3x}\,\dot{x}_3. \tag{25}$$

$$Q_{\mathrm{d}.7} = \delta_4\left(\dot{\varphi}_3 - \dot{\varphi}_2\right) - \delta_2\left(\dot{\varphi}_2 - \dot{\varphi}_1\right). \tag{26}$$

$$Q_{\mathrm{d}.8} = \delta_1\left(\dot{\varphi}_0 - \dot{\varphi}_1\right) + \delta_2\left(\dot{\varphi}_2 - \dot{\varphi}_1\right). \tag{27}$$

$$Q_{\mathrm{d}.9} = -d_{6z}\,\dot{z}_6. \tag{28}$$

$$Q_{\mathrm{d}.10} = -\delta_5\left(\dot{\varphi}_4 - \dot{\varphi}_2\right). \tag{29}$$

$$Q_{\text{ar5.1}} = -d_{\text{ar5}}\,\nu_5\left[\ -\sin(\varphi_3)\dot{X}_5 + \cos(\varphi_3)\dot{Y}_5 + \frac{\eta\,\dot{Z}_5}{\sqrt{-\eta^2-\xi^2+L_0{}^2}}\ \right]. \tag{30}$$

$$Q_{\text{ar5.2}} = -d_{\text{ar5}}\,\nu_5\left[\ \cos(\varphi_3)\dot{X}_5 + \sin(\varphi_3)\dot{Y}_5 + \frac{\xi\,\dot{Z}_5}{\sqrt{-\eta^2-\xi^2+L_0{}^2}}\ \right]. \tag{31}$$

$$Q_{\text{ar5.3}} = -d_{\text{ar5}}\,\nu_5\,\dot{Z}_5. \tag{32}$$

$$Q_{\text{ar5.4}} = d_{\text{ar5}}\,\nu_5\left[\ \eta\left(\cos(\varphi_3)\dot{X}_5 + \sin(\varphi_3)\dot{Y}_5\right) + \xi\left(\sin(\varphi_3)\dot{X}_5 - \cos(\varphi_3)\dot{Y}_5\right) + R_0\left(\sin(\varphi_3)\dot{X}_5 - \cos(\varphi_3)\dot{Y}_5\right)\ \right]. \tag{33}$$

$$Q_{\text{ar5.5}} = d_{\text{ar5}}\,\nu_5\left(\sin(\varphi_2)\dot{X}_5 - \cos(\varphi_2)\dot{Y}_5\right). \tag{34}$$

$$Q_{\text{ar5.6}} = -d_{\text{ar5}}\,\nu_5\left[\ \cos(\varphi_2)\dot{X}_5 + \sin(\varphi_2)\dot{Y}_5 - \frac{2R_0\,\dot{Z}_5}{H_0}\ \right]. \tag{35}$$

$$Q_{\text{ar5.7}} = d_{\text{ar5}}\,\nu_5\left[\ y_3\left(\cos(\varphi_2)\dot{X}_5 + \sin(\varphi_2)\dot{Y}_5\right) + x_3\left(\sin(\varphi_2)\dot{X}_5 - \cos(\varphi_2)\dot{Y}_5\right)\ \right]. \tag{36}$$

The generalised non-conservative forces represent the dissipative effects in the mathematical model. There is one generalised force for each degree of freedom of the model, and it is defined as the sum of the contributions:

$$Q_j' = Q_{\text{ar5.}j} + Q_{\text{d.}j} + Q_{\text{FR.}j} \quad \text{for } j=1,\ \ldots,\ 10. \tag{37}$$

The components introduced by Eqs. (15), (16) and (37) were appropriately treated, and the derivatives (where appropriate) were calculated. The corresponding expressions were then substituted into Eq. (1). After rearranging the equation, the system of differential equations of motion of the studied mathematical model was derived. This system can be represented in matrix form:

$$\begin{bmatrix} A_{11} & A_{12} & A_{13} & A_{14} & A_{15} & A_{16} & A_{17} & 0 & 0 & 0 \\ A_{21} & A_{22} & A_{23} & A_{24} & A_{25} & A_{26} & A_{27} & 0 & 0 & 0 \\ A_{31} & A_{32} & A_{33} & 0 & 0 & A_{36} & 0 & 0 & 0 & 0 \\ A_{41} & A_{42} & 0 & A_{44} & A_{45} & A_{46} & A_{47} & 0 & 0 & 0 \\ A_{51} & A_{52} & 0 & A_{54} & A_{55} & 0 & A_{57} & 0 & A_{59} & 0 \\ A_{61} & A_{62} & A_{63} & A_{64} & 0 & A_{66} & A_{67} & 0 & A_{69} & A_{610} \\ A_{71} & A_{72} & 0 & A_{74} & A_{75} & A_{76} & A_{77} & 0 & A_{79} & 0 \\ 0 & 0 & 0 & 0 & 0 & 0 & 0 & A_{88} & 0 & 0 \\ 0 & 0 & 0 & 0 & A_{95} & A_{96} & A_{97} & 0 & A_{99} & 0 \\ 0 & 0 & 0 & 0 & 0 & A_{106} & 0 & 0 & 0 & A_{1010} \end{bmatrix} \cdot \begin{bmatrix} \ddot{\eta} \\ \ddot{\xi} \\ \ddot{z}_4 \\ \ddot{\varphi}_3 \\ \ddot{y}_3 \\ \ddot{x}_3 \\ \ddot{\varphi}_2 \\ \ddot{\varphi}_1 \\ \ddot{\varphi}_4 \\ \ddot{z}_6 \end{bmatrix} = \begin{bmatrix} R_1 \\ R_2 \\ R_3 \\ R_4 \\ R_5 \\ R_6 \\ R_7 \\ R_8 \\ R_9 \\ R_{10} \end{bmatrix} \tag{38}$$

where the vector components R_j and the elements A_{jk} are defined in Appendix. Eq. (38) represents a system of ten second-order non-linear differential equations with non-constant coefficients. This system was solved numerically using the fourth-order Runge-Kutta method.

3 The measurements

In order to confirm the mathematical model, the results of measurements from prior researches [*x*, *y*, *z*] are used. A short description of an experimental setup is introduced for convenience. A laboratory sized slewing crane is shown in Fig. 2. A three-phase squirrel-cage electric motor is the driving motor, and a computer controlled frequency controller is used to regulate its rotation speed.

The crane model is equipped with sensors for measuring seven different quantities as follows. The radial and tangential angles (α_R and α_T in Fig. 1) of the pendulum motion were measured using two inductive transducers (MP 1 and MP 2 in Fig. 2). The bending moments on the jib, around the *y*- and *z*-axis, were measured using strain gauges on the jib (MP 3 and 4 in Fig. 2). In addition, the torsion moment on the torsion shaft was measured with strain gauges (MP 5 in Fig. 2). The angles of rotation of the driving shaft (MP 7) and of the slewing platform (MP 6 in Fig. 2) were measured with incremental rotary encoders.

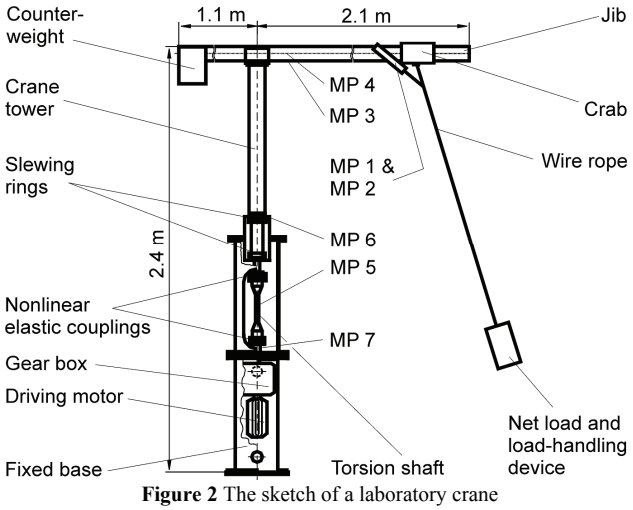

Figure 2 The sketch of a laboratory crane

4 Results of the simulation and comparison with measurements

The developed multi-mass dynamic model was used for the simulation. To enable the verification of the developed model, the comparison with measured results

was necessary. To allow this comparison, the corresponding data from the physical model of a slewing crane were used as input data for the simulation.

The following crane's working-cycle was simulated. The acceleration of the slewing motion of the crane platform from zero to the maximum angular velocity $\dot{\varphi}_{0,\max}$ in time t_1 was followed by the rotation of the platform with constant angular velocity in duration of time t_2. At the end of the rotation, the deceleration of the rotation from the existing constant angular velocity to zero in time t_3 was applied and finally the phase of observation of the crane after the stopping of the rotation in duration of time t_4 was enabled. A payload was suspended from the jib during the entire cycle.

Table 1 Selected values of the acceleration time t_1

	Example 1	Example 2	Example 3	Example 4	Example 5	Example 6
t_1(s) =	$t_Q/4$= 0,71	$2t_Q/4$ = 1,42	$3t_Q/4$= 2,13	t_Q = 2,84	$5t_Q/4$ = 3,55	$6t_Q/4$ = 4,26

Table 2 Values of the other parameters

Parameter	Value	Description
t_1	see Tab. 1	Acceleration time of the slewing motion
t_2	6 s	*Time of rotation with constant angular velocity* (8 s for Examples 1, 2)
t_3	= t_1	Deceleration time of the slewing motion
t_4	different	Time of observation after stopping the rotation of the platform
$t_1+t_2+t_3+t_4$	25 s	Total time of the observation of the phenomenon
$\dot{\varphi}_{0,\max}$	0,738 rad/s	Angular velocity of the rotation of the platform for Examples 1 to 6
m_Q	50 kg	Mass of the payload of the laboratory crane
R_0	2 m	Radial position of the load suspension point on the crane arm
L_0	2 m	Length of the free end of the load bearing steel rope
acceleration/ deceleration type	constant	Constant value of the angular acceleration/deceleration during all acceleration/deceleration time

The simulations were carried out with a range of load masses (m_Q = 20 to 50 kg), different radii of the suspension point (R_0 = 1 to 2 m), and different lengths of the load-carrying rope (L_0 = 0,5 to 2 m). The effects of the various types of acceleration and deceleration on the trajectory of the suspended load were also studied, including the changes to the acceleration time and the average acceleration. The results for four examples, defined by tables 1 and 2, are shown in Figs. 3 to 18.

The acceleration time of the payload suspension point in relation with the natural frequency/period of oscillation of the suspended payload has a strong influence on the payload sway after the acceleration [25]. From the chosen length of the load-carrying rope L_0 = 2 m, the period of oscillation of the suspended payload, looked at as a mathematical pendulum, can be calculated as t_Q = 2,84 s.

From Figs. 3 and 4 the pendulum motion of the suspended payload for Example 1 can be seen. Figures 5 to 7 introduce the crane's dynamic loading and Fig. 8 introduces the angle of rotation of a slewing platform. In these Figures, and in Figs. 9 to 18, the thin black continuous line represents the graph of measured values, whereas the bold black continuous line represents the results of the simulation. The graph representing the angle φ_0 of rotation of the driving shaft is shown with grey continuous line of a medium thickness, introducing the phases of the input angular velocity $\dot{\varphi}_0(t)$.

In Fig. 3 the tangential angle α_T of the load sway is introduced, which can be compared with the in-plane load sway during the translation of the payload's suspension point. In the acceleration phase, a degree of payload lag can be observed. The maximum negative value of α_T (payload lag) during the rotation is observed immediately after the acceleration phase. The simulated value of this maximum is 14,9 % greater than the measured one.

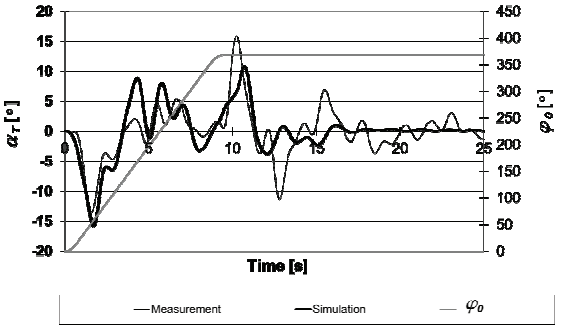

Figure 3 Tangential (α_T) angle of the load sway with respect to time for Example 1

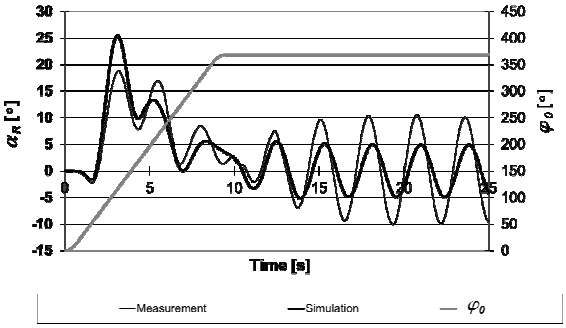

Figure 4 Radial (α_R) angle of the load sway with respect to time for Example 1

The phase of moving with a constant speed is denoted by oscillations, the mean value of which is positive but close to the static equilibrium. In the deceleration phase, the payload starts to forestall the suspension point. After the rotation stops, the positive angle keeps increasing until the maximum positive peak value is reached. The

simulated value of this peak is for 35,0 % lower than the measured value. Such a difference is caused by large nonlinearity of the observed phenomenon where even small differences in conditions at the beginning of the deceleration phase lead to bigger later deviations. Finally, damped oscillations around the static equilibrium are developed. Comparison of the curves in the graph shows that the qualitative matching of the simulated and measured results is very good during acceleration, constant velocity rotation and even a few seconds after the stop of the rotation.

In Fig. 4 the radial angle α_R of the load sway is introduced, which is unique to slewing cranes. This angle is initially mainly a consequence of the centrifugal force due to the rotation of the crane. Additionally, in the first moment of the acceleration phase, an apparent shift of the payload in the radial direction is encountered toward the centre of rotation (a negative value of α_R). This is the result of the rotation of the local coordinate system $\xi\eta\zeta$ and of the movement of its origin (see Fig. 1), which is located at the payload's suspension point. This effect is noticeable in the measured and in the simulated cases. The difference in the peak values is 19,6 % (only 0,33°).

The oscillations in radial direction (α_R) are influenced also by tangential oscillations (α_T) and vice versa and are therefore coupled. They describe a complex spatial pendulum motion of a payload. The positive peak value of the radial angle (α_R) is achieved in the phase of rotation with constant speed. The comparison shows that the simulated peak value is about 37 % higher than the measured one. The quantitative difference of these two values is rather big. On the other hand, the overall qualitative and quantitative agreement is very good. The comparison shows that there is no phase shift between the simulated and measured curves.

The bending moment in the jib around the z-axis M_h (generating deformation of the jib in the horizontal plane xy) is shown in Fig. 5, and the torsion moment in the driving shaft M_t is shown in Fig. 7. The graphs for both moments are similar because they are both caused by horizontal inertial forces acting in a tangential direction. A good qualitative agreement of the curves is observed. A quantitative agreement is better during first three observation phases. The difference becomes more noticeable during the fourth phase. The simulated results show higher values of the moments in comparison with the measurements and are therefore of a conservative nature.

The bending moment in the jib around the y-axis M_V (generating deformation of the jib in the vertical plane xz) is shown in Fig. 6. Its mean value is defined by the weight of the payload and some parts of the crane. The oscillation of its value with respect to time is a consequence of the dynamic effects of the payload's spatial sway in the foreground. A good qualitative and quantitative agreement between the curves is clear from the graph. In Fig. 8 graphs of angle of rotation of a slewing platform φ_1 are presented together with the graph of driving shaft rotation. The acceleration of the slewing platform begins after the acceleration of the driving shaft is already finished, because of the elasticity of the non-linear elastic couplings, mounted on the torsion shaft (see Fig. 2). The acceleration of the rotation of the platform is higher in the simulated case than in the measured case because of the representation of the non-linear stiffness characteristic in the mathematical model. It is presented by means of three straight lines instead of a smooth curve.

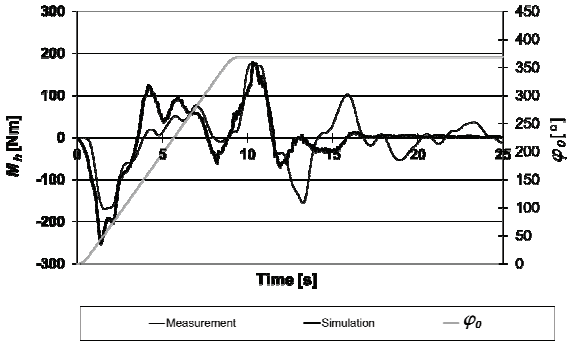

Figure 5 Bending moment in the jib around the z-axis (M_h) for Example 1

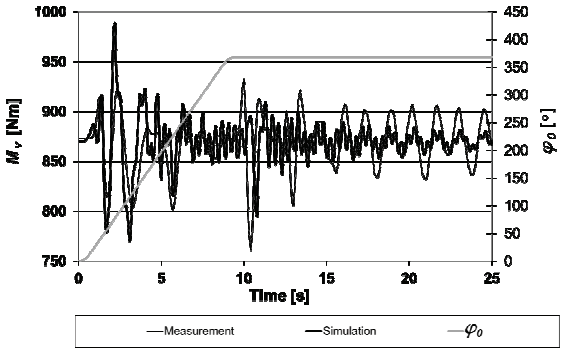

Figure 6 Bending moment in the jib around the y-axis (M_v) for Example 1

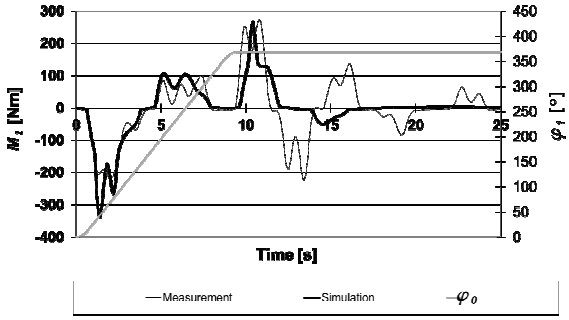

Figure 7 Torsion moment in the driving shaft (M_t) for Example 1

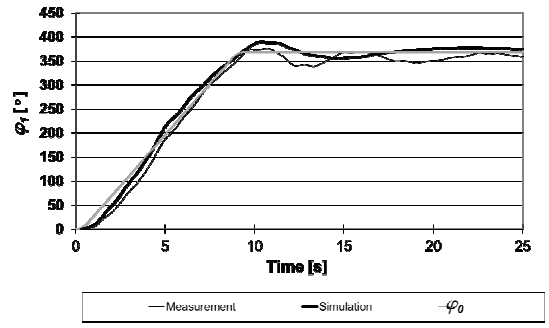

Figure 8 Angle of rotation of the crane slewing platform (φ_1) for Example 1

Higher acceleration of the rotation has influence on the further course of simulation. It is the reason for higher leg of the tangential angle of load sway (α_T) which

furthermore results in higher values of the dynamic loading. Because of the value of the leg in the simulated case is higher, also the subsequent peak value of the (coupled) radial angle of the load sway (α_R) is higher.

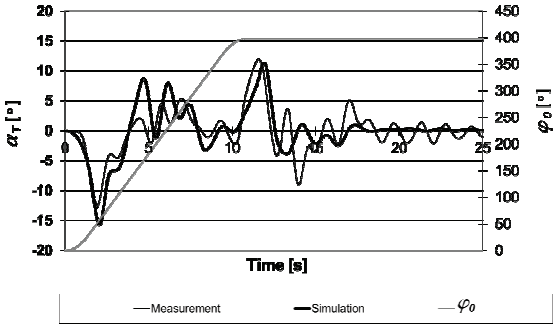

Figure 9 Tangential (α_T) angle of the load sway with respect to time for Example 2

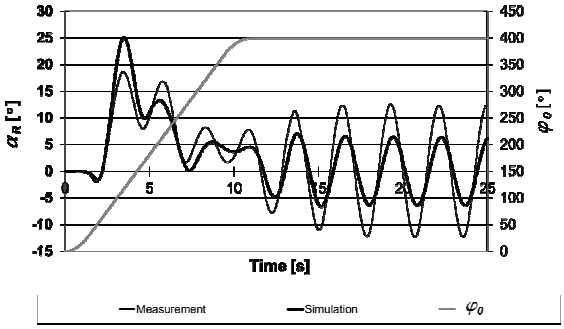

Figure 10 Radial (α_R) angle of the load sway with respect to time for Example 2

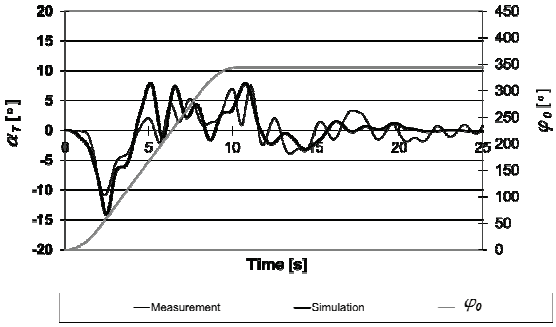

Figure 11 Tangential (α_T) angle of the load sway with respect to time for Example 3

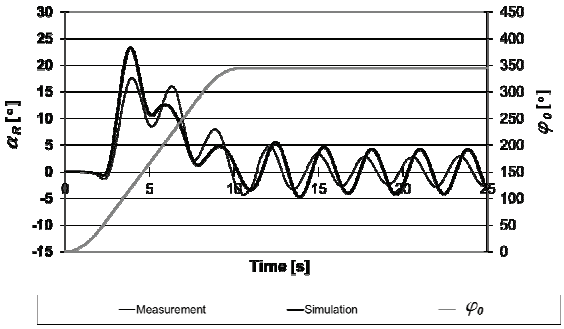

Figure 12 Radial (α_R) angle of the load sway with respect to time for Example 3

For Examples 2 to 6 only graphs of angles (α_T) and (α_R) of the load sway with respect to time are shown, which are of the most interest at this point. A good qualitative agreement of the results is supplemented by a good quantitative agreement, which is in most cases better than in Example 1. The same remarks are valid also for non-shown diagrams of torsion and bending moments.

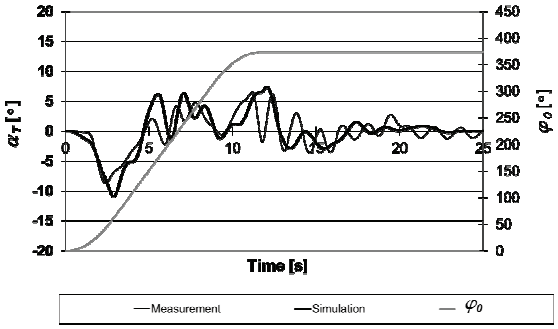

Figure 13 Tangential (α_T) angle of the load sway with respect to time for Example 4

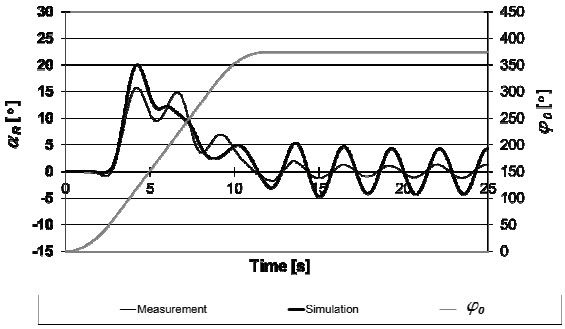

Figure 14 Radial (α_R) angle of the load sway with respect to time for Example 4

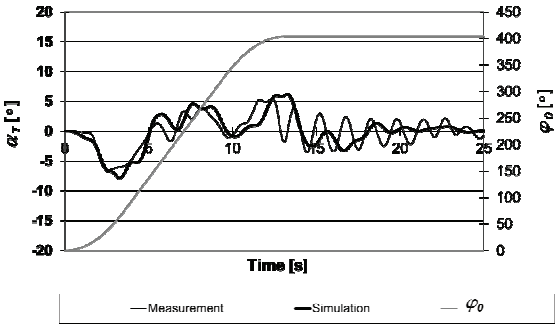

Figure 15 Tangential (α_T) angle of the load sway with respect to time for Example 5

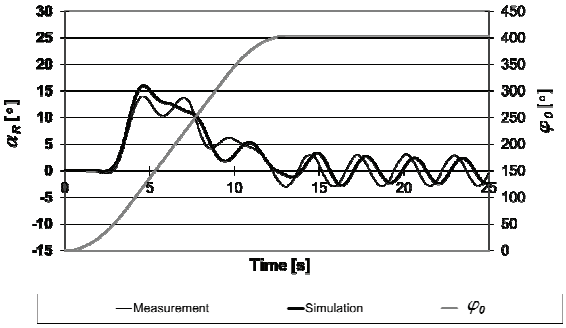

Figure 16 Radial (α_R) angle of the load sway with respect to time for Example 5

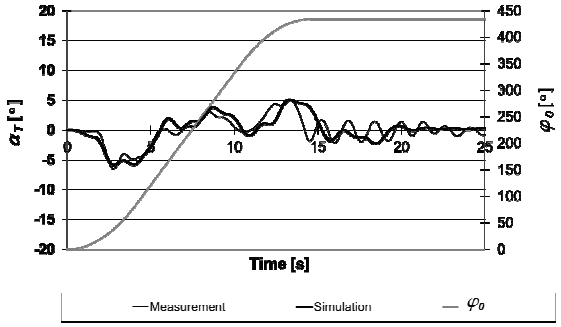

Figure 17 Tangential (α_T) angle of the load sway with respect to time for Example 6

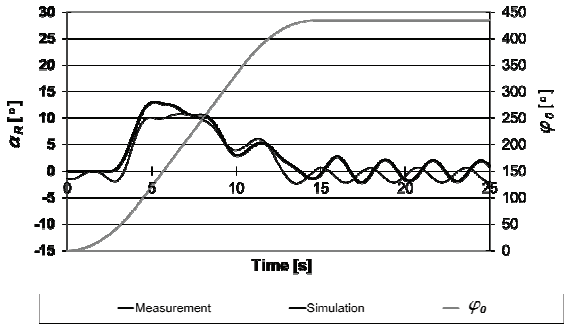

Figure 18 Radial (α_R) angle of the load sway with respect to time for Example 6

5 Conclusions

In the paper, a mathematical model of a slewing crane during slewing motion with 6 mass elements and with 10 degrees of freedom is presented. Two mass moments of inertia and four point masses are used enabling a realistic mathematical description of this real-world problem. To restrain the number of degrees of freedom of the model, a few of the less significant influences are neglected. Lagrange equations were used to derive the equations of motion, and a computer program was developed to solve these equations. The mathematical model has no restrictions in terms of small angles of the load sway. This makes it possible to study the crane's behaviour under extreme conditions, as is the case in the examples shown, where the values of the radial angle (α_R) go up to 26°.

For the purpose of the validation of the mathematical model, extensive measurements were carried out on the laboratory crane. A detailed comparison was carried out between the measured results and the results of the simulation. A very good qualitative and good quantitative matching of the results was established. The agreement of the results remains good during the deceleration phase. This confirms that the initial conditions for the deceleration phase, which are calculated at the end of the previous phase of the rotation, are precise enough to ensure the accurate continuation of the simulation. In the phase of stand still sometimes a phase shift or amplitude differences become more noticeable for the reason of multiplication of deviations of this highly nonlinear mathematical model.

The simulated loadings are conservative in nature, because they are very close to or higher than the measured loads in majority of investigated cases. This is important for fatigue assessment of the real-world crane's structure where the developed mathematical model can be used for loading spectra prediction.

The presented model accounts for the mass inertia of all the most pointed out masses including the mass of the counterweight, which is bolted at majority of the cranes. Further improvement of the simulation results can be expected if the non-linear stiffness and damping characteristics of the elastic couplings are defined in more details

6 References

[1] Feng, J.; Yoo, S. C. Dynamic Analysis of Tower Cranes. // Journal of Engineering Mechanics, 131, 1(2005), pp. 88-96.

[2] Jerman, B.; Podržaj, P.; Kramar, J. An Investigation of Slewing-Crane Dynamics During Slewing Motion - Development and Verification of a Mathematical Model. // International Journal of Mechanical Sciences, 46, 5(2004), pp. 729-750.

[4] Mitrović, N.; Kostić, V.; Petronijević, M.; Jeftenić, B. Practical Implementation of Load Sharing and Anti Skew Controllers for Wide Span Gantry Crane Drives. // Strojniški vestnik - Journal of Mechanical Engineering, 56, 3(2010), pp. 207-216.

[5] Maksimović, K.; Nikolić-Stanojević, V.; Maksimović, S.; Stupar, S.; Vasović, I. Fatigue Life Estimation of Notched Structural Components. // Strojniški vestnik - Journal of Mechanical Engineering, 56, 12(2010), pp. 846-852.

[3] Abdel-Rahman, E. M.; Nayfeh, A. H.; Masoud, Z. N. Dynamics and Control of Cranes: A Review. // Journal of Vibration and Control, 9, 7(2003), pp. 863-908.

[6] Lee, H. A new design approach for the anti-swing trajectory control of overhead cranes with high-speed hoisting. // International Journal of Control, 77, 10(2004), pp. 931-940.

[7] Yavin, Y.; Kemp, P. D. The application of extended inverse dynamics control. // Computers and Mathematics with Applications, 40, 4-5(2000), pp. 669-677.

[8] Spathopoulos, M. P.; Fragopoulos, D. Pendulation control of an offshore crane. // International Journal of Control, 77, 7 (2004), pp. 654-670.

[9] Glossiotis, G.; Antoniadis, I. Payload sway suppression in rotary cranes by digital filtering of the commanded inputs. // Proceedings of the Institution of Mechanical Engineers, Part K, Journal of Multi-body Dynamics, 217, 2(2003), pp. 99-109.

[10] Ghigliazza, R. M.; Holmes, P. On the dynamics of cranes, or spherical pendula with moving supports. // Int. J. of Non-Linear Mechanics, 37, 7(2002), pp. 1211-1221.

[11] Matthias, K.; Kirsten, N. Dynamische beanspruchung im dreh - und wippwek von doppellenker - wippdrehkranen - Teil 2. // Hebezeuge und Fördermittel, 10, (1984), pp. 303-305.

[12] Cartmell, M. P.; Morrish, L.; Taylor, A. J. Dynamics of Spreader Motion in a Gantry Crane. // Proceedings of the Institution of Mechanical Engineers, Part C, Journal of Mechanical Engineering Science, 212, 2(1998), pp. 85-105.

[13] Lee, J.-W.; Kim, D.-H. Dynamics of a spreader suspended by four flexible cables. // Proceedings of the Institution of Mechanical Engineers, Part C, Journal of Mechanical Engineering Science, 218, 10(2004), pp. 1125-1138.

[14] Lee, J.-W.; Kim, D.-H.; Oh, J.-H. A unified approach to the kinematics of a spreader suspended by multiple cables. // Proceedings of the Institution of Mechanical Engineers, Part C, Journal of Mechanical Engineering Science, 217,

3(2003), pp. 289-312.
[15] Oguamanam, D. C. D.; Hansen, J. S. Dynamics of a three-dimensional overhead crane system. // Journal of Sound and Vibration, 242, 3(2001), pp. 411-426.
[16] Wu, J. J.; Whittaker A. R.; Cartmell, M. P. The use of finite element techniques for calculating the dynamic response of structures to moving loads. // Computers and Structures, 78, 6(2000), pp. 789-799.
[17] Zrnić, N.; Hoffmann, K.; Bošnjak, S. Modelling of Dynamic Interaction between Structure and Trolley for Mega Container Cranes. // Mathematical and Computer Modelling of Dynamical Systems, 15, 3(2009), pp. 295-311.
[18] Zrnić, N.; Bošnjak, S.; Hoffmann, K. Parameter sensitivity analysis of non-dimensional models of quayside container cranes. // Mathematical and Computer Modelling of Dynamical Systems, 16, 2(2010), pp. 145-160.
[19] Zrnić, N.; Gašić, V.; Obradović, A.; Bošnjak, S. Appropriate modeling of dynamic behavior of quayside container cranes boom under a moving trolley. // Springer Proceedings in Physics 139, Vibration problems ICOVP 2011, pp. 81-86, 2011, Springer.
[20] Gašić, V.; Zrnić, N.; Obradović, A.; Bošnjak, S. Consideration of Moving Oscillator Problem in Dynamic Responses of Bridge Cranes. // FME Transactions, 39, 1(2011), pp. 17-24.
[21] Vladić, J.; Đokić, R.; Kljajin, M.; Karakašić, M. Modelling and simulations of elevator dynamic behaviour (Preliminary notes). // Tehnički vjesnik - Technical Gazette, 18, 3(2011), pp. 423-434.
[22] Draganić, H.; Hadzima-Nyarko, M.; Morić, D. Comparison of RC frames periods with the empiric expressions given in Eurocode 8 (Subject reviews). // Tehnički vjesnik - Technical Gazette, 17, 1(2010), pp. 93-100.
[23] Jerman, B. An enhanced mathematical model for investigating the dynamic loading of a slewing crane. // Proc. Inst. Mech. Eng., C J. mech. eng. sci., 220, 4(2006), pp. 421-433.
[24] Jerman, B.; Kramar, J. A study of the horizontal inertial forces acting on the suspended load of slewing cranes. // Int. j. mech. sci. [Print ed.], 50, 3(2008), pp. 490-500.
[25] Strip, D. R. Swing-Free Transport of Suspended Objects: A General Treatment. // IEEE Transactions on Robotics and Automation, 5, 2(1989), pp. 234-236.
[26] Gašić, V.; Zrnić, N.; Rakin, M. Consideration of a moving mass effect on dynamic behaviour of a jib crane structure. // Technical Gazette, 19, 1(2012), pp. 115-121.

Authors' addresses

mr. sc. Ivica Marinović
Fund for Vocational Rehabilitation and Employment of Persons with Disabilities
Vilsonovo šetalište 10
71000 Sarajevo, B&H
E-mail: ivica-marinovic@hotmail.com

assoc. prof. dr. Denijal Sprečić
University of Tuzla,
Faculty of Mechanical Engineering,
Univerzitetska 4
75000 Tuzla, B&H.
E-mail: denijal.sprecic@untz.ba

assist. prof. dr. Boris Jerman
University of Ljubljana,
Faculty of Mechanical Engineering,
Aškerčeva c. 6
1000 Ljubljana, Slovenia
E-mail: boris.jerman@fs.uni-lj.si

7 Appendix

The vector components R_j:

$$R_1 = m_5\left\{\dot{\varphi}_3\left((\dot{y}_3 + x_3\dot{\varphi}_2)(\varphi_3-\varphi_2) + (y_3\dot{\varphi}_2 - \dot{x}_3) - (\dot{\xi} - \eta\dot{\varphi}_3)\right) - g\frac{\eta}{\sqrt{L_0^2-\xi^2-\eta^2}} + \right.$$
$$\left. + \frac{\dot{z}_4[\dot{\eta}(L_0^2-\xi^2)+\xi\dot{\xi}\eta]}{\sqrt{(L_0^2-\xi^2-\eta^2)^3}} + \frac{(\xi\dot{\xi}+\eta\dot{\eta})[\dot{\eta}(L_0^2-\xi^2)+\xi\dot{\xi}\eta]}{(L_0^2-\xi^2-\eta^2)^2} - \frac{2R_0\dot{x}_3}{H_0}\frac{\dot{\eta}(L_0^2-\xi^2)+\xi\dot{\xi}\eta}{\sqrt{(L_0^2-\xi^2-\eta^2)^3}}\right\} -$$
$$- d_{ar5}v_5\left\{\dot{x}_3(\varphi_2-\varphi_3) + \dot{y}_3 + [x_3 - y_3(\varphi_2-\varphi_3)]\dot{\varphi}_2 + (R_0+\xi)\dot{\varphi}_3 + \dot{\eta} + \frac{\eta}{\sqrt{L_0^2-\xi^2-\eta^2}}\left[\dot{z}_4 + \frac{\xi\dot{\xi}+\eta\dot{\eta}}{\sqrt{L_0^2-\xi^2-\eta^2}} - \frac{2R_0}{H_0}\dot{x}_3\right]\right\}$$

$$R_2 = m_5\left\{\dot{\varphi}_3\left((y_3\dot{\varphi}_2 - \dot{x}_3)(\varphi_3-\varphi_2) + (\dot{y}_3 + x_3\dot{\varphi}_2) + (R_0+\xi)\dot{\varphi}_3 + \dot{\eta}\right) - g\frac{\xi}{\sqrt{L_0^2-\xi^2-\eta^2}} + \right.$$
$$\left. + \frac{\dot{z}_4[\dot{\xi}(L_0^2-\eta^2)+\eta\dot{\eta}\xi]}{\sqrt{(L_0^2-\xi^2-\eta^2)^3}} + \frac{(\xi\dot{\xi}+\eta\dot{\eta})[\dot{\xi}(L_0^2-\eta^2)+\eta\dot{\eta}\xi]}{(L_0^2-\xi^2-\eta^2)^2} - \frac{2R_0\dot{x}_3}{H_0}\frac{\dot{\xi}(L_0^2-\eta^2)+\eta\dot{\eta}\xi}{\sqrt{(L_0^2-\xi^2-\eta^2)^3}}\right\} -$$
$$- d_{ar5}v_5\left\{\dot{x}_3 + \dot{y}_3(\varphi_3-\varphi_2) + [x_3(\varphi_3-\varphi_2) - y_3]\dot{\varphi}_2 + (\dot{\xi} - \eta\dot{\varphi}_3) + \frac{\xi}{\sqrt{L_0^2-\xi^2-\eta^2}}\left[\dot{z}_4 + \frac{\xi\dot{\xi}+\eta\dot{\eta}}{\sqrt{L_0^2-\xi^2-\eta^2}} - \frac{2R_0}{H_0}\dot{x}_3\right]\right\}$$

$$R_3 = -g(m_4+m_5) - k_{4z}z_4 - d_{4z}\dot{z}_4 - d_{ar4}v_4\left[\dot{z}_4 - \frac{2R_0}{H_0}\dot{x}_3\right] - d_{ar5}v_5\left\{\dot{z}_4 + \frac{\xi\dot{\xi}+\eta\dot{\eta}}{\sqrt{L_0^2-\xi^2-\eta^2}} - \frac{2R_0}{H_0}\dot{x}_3\right\}$$

$$R_4 = -\left\{(m_4+m_5)\left[R_0\dot{\varphi}_3(\dot{x}_3 - y_3\dot{\varphi}_2)\right] + m_5\left[(\dot{x}_3 - y_3\dot{\varphi}_2)(\dot{\eta}+\xi\dot{\varphi}_3) + (\dot{y}_3 + x_3\dot{\varphi}_2)(\dot{\xi} - \eta\dot{\varphi}_3)\right]\right\} - \kappa_4(\varphi_3-\varphi_2) + \kappa_5(\varphi_4-\varphi_3) -$$
$$- \delta_4(\dot{\varphi}_3 - \dot{\varphi}_2) - \delta_5(\dot{\varphi}_4 - \dot{\varphi}_3) - d_{ar4}v_4R_0\left[(\dot{x}_3 - y_3\dot{\varphi}_2)(\varphi_2-\varphi_3) + (\dot{y}_3 + x_3\dot{\varphi}_2) + R_0\dot{\varphi}_3\right] -$$
$$- d_{ar5}v_5\left\{\left[(R_0+\xi)(\varphi_2-\varphi_3) - \eta\right](\dot{x}_3 - y_3\dot{\varphi}_2) + \left[(R_0+\xi) - \eta(\varphi_3-\varphi_2)\right](\dot{y}_3 + x_3\dot{\varphi}_2) + \left[(R_0+\xi)^2 + \eta^2\right]\dot{\varphi}_3 + (R_0+\xi)\dot{\eta} - \eta\dot{\xi}\right\}$$

$$R_5 = -\dot{\varphi}_2\left\{\left[(m_3+m_4+m_5+m_6)(\dot{x}_3 - y_3\dot{\varphi}_2) + (m_4+m_5)R_0\dot{\varphi}_3(\varphi_2-\varphi_3)\right] + m_5\left[(\dot{\eta}+\xi\dot{\varphi}_3)(\varphi_2-\varphi_3) + (\dot{\xi}-\eta\dot{\varphi}_3)\right] + m_6P_0\dot{\varphi}_4(\varphi_4-\varphi_2)\right\} -$$
$$-k_{3y}y_3 - d_{3y}\dot{y}_3 - d_{ar3}v_3(\dot{y}_3 + x_3\dot{\varphi}_2) - d_{ar4}v_4\left[(\dot{y}_3 + x_3\dot{\varphi}_2) + R_0\dot{\varphi}_3\right] - d_{ar5}v_5\left\{\dot{y}_3 + x_3\dot{\varphi}_2 + \left[(R_0+\xi) - \eta(\varphi_3-\varphi_2)\right]\dot{\varphi}_3 + \dot{\eta} + \dot{\xi}(\varphi_3-\varphi_2)\right\} -$$
$$- d_{ar6}v_6\left\{\dot{y}_3 + x_3\dot{\varphi}_2 - P_0\dot{\varphi}_4\right\}$$

$$R_6 = \dot{\varphi}_2\left\{(m_3+m_4+m_5+m_6)(\dot{y}_3 + x_3\dot{\varphi}_2) + (m_4+m_5)R_0\dot{\varphi}_3 + m_5\left[(\dot{\xi}-\eta\dot{\varphi}_3)(\varphi_2-\varphi_3) + (\dot{\eta}+\xi\dot{\varphi}_3)\right] - m_6P_0\dot{\varphi}_4\right\} -$$
$$-\frac{2g}{H_0}\left[m_6P_0 - (m_4+m_5)R_0\right] - k_{3x}x_3 - d_{3x}\dot{x}_3 - d_{ar3}v_3(\dot{x}_3 - y_3\dot{\varphi}_2) - d_{ar4}v_4\left[(\dot{x}_3 - y_3\dot{\varphi}_2) + R_0\dot{\varphi}_3(\varphi_2-\varphi_3) - \frac{2R_0}{H_0}\left(\dot{z}_4 - \frac{2R_0}{H_0}\dot{x}_3\right)\right] -$$
$$- d_{ar5}v_5\left\{\dot{x}_3 - y_3\dot{\varphi}_2 + \left[(R_0+\xi)(\varphi_2-\varphi_3) - \eta\right]\dot{\varphi}_3 + \dot{\eta}(\varphi_2-\varphi_3) + \dot{\xi} - \frac{2R_0}{H_0}\left[\dot{z}_4 + \frac{\xi\dot{\xi}+\eta\dot{\eta}}{\sqrt{L_0^2-\xi^2-\eta^2}} - \frac{2R_0}{H_0}\dot{x}_3\right]\right\} -$$
$$- d_{ar6}v_6\left\{\dot{x}_3 - y_3\dot{\varphi}_2 + P_0(\varphi_4-\varphi_2)\dot{\varphi}_4 + \frac{2P_0}{H_0}\dot{z}_6 + \frac{4P_0^2}{H_0^2}\dot{x}_3\right\}$$

$$R_7 = (m_4+m_5)R_0\dot{\varphi}_3(\dot{x}_3 - y_3\dot{\varphi}_2) + m_5\left[(\dot{x}_3 - y_3\dot{\varphi}_2)(\dot{\eta}+\xi\dot{\varphi}_3) + (\dot{y}_3 + x_3\dot{\varphi}_2)(\dot{\xi}-\eta\dot{\varphi}_3)\right] - m_6P_0\dot{\varphi}_4(\dot{x}_3 - y_3\dot{\varphi}_2) -$$
$$-\kappa_2(\varphi_2-\varphi_1) + \kappa_4(\varphi_3-\varphi_2) - \delta_2(\dot{\varphi}_2-\dot{\varphi}_1) - \delta_4(\dot{\varphi}_3-\dot{\varphi}_2) - d_{ar3}v_3\left[\dot{\varphi}_2(x_3^2+y_3^2) + (\dot{y}_3x_3 - \dot{x}_3y_3)\right] -$$
$$- d_{ar4}v_4\left\{\dot{\varphi}_2(x_3^2+y_3^2) + (\dot{y}_3x_3 - \dot{x}_3y_3) + R_0\dot{\varphi}_3\left[x_3 - y_3(\varphi_2-\varphi_3)\right]\right\} -$$
$$-d_{ar5}v_5\left\{(x_3^2+y_3^2)\dot{\varphi}_2 + (x_3\dot{y}_3 - y_3\dot{x}_3) + \left[(R_0+\xi)\left[y_3(\varphi_3-\varphi_2)+x_3\right] + \eta\left[y_3 - x_3(\varphi_3-\varphi_2)\right]\right]\dot{\varphi}_3 + \left[x_3 + y_3(\varphi_3-\varphi_2)\right]\dot{\eta} + (x_3(\varphi_3-\varphi_2) - y_3)\dot{\xi}\right\} -$$
$$- d_{ar6}v_6\left\{(x_3^2+y_3^2)\dot{\varphi}_2 + (x_3\dot{y}_3 - \dot{x}_3y_3) - P_0\left[x_3 + y_3(\varphi_4-\varphi_2)\right]\dot{\varphi}_4\right\}$$

$$R_8 = \kappa_2(\varphi_2-\varphi_1) - \kappa_1(\varphi_1-\varphi_0) - M_{FR} - \delta_1(\dot{\varphi}_1-\dot{\varphi}_0) - \delta_2(\dot{\varphi}_2-\dot{\varphi}_1)$$

$$R_9 = m_6P_0\dot{\varphi}_4(\dot{x}_3 - y_3\dot{\varphi}_2) - \kappa_5(\varphi_4-\varphi_3) - \delta_5(\dot{\varphi}_4-\dot{\varphi}_3) - d_{ar6}v_6P_0\left\{P_0\dot{\varphi}_4 - \left[x_3 + y_3(\varphi_4-\varphi_2)\right]\dot{\varphi}_2 + \dot{x}_3(\varphi_4-\varphi_2) - \dot{y}_3\right\}$$

$$R_{10} = -gm_6 - k_{6z}z_6 - d_{5z}\dot{z}_6 - d_{ar6}v_6\left\{\dot{z}_6 + \frac{2P_0}{H_0}\dot{x}_3\right\}$$

The elements A_{jk} of the mass matrix. (*The order in the table is chosen so, that the space used is minimised.*)

$A_{11} = m_5\left(1+\frac{\eta^2}{\zeta^2}\right)$	$A_{16} = -m_5\left((\varphi_3-\varphi_2) + \frac{2R_0\eta}{H_0\zeta}\right)$	$A_{21} = m_5\left(\frac{\eta\xi}{\zeta^2}\right)$	$A_{22} = m_5\left(1+\frac{\xi^2}{\zeta^2}\right)$
$A_{12} = m_5\left(\frac{\eta\xi}{\zeta^2}\right)$	$A_{36} = -\left(\frac{(m_4+m_5)2R_0}{H_0}\right)$	$A_{23} = m_5\left(\frac{\xi}{\zeta}\right)$	$A_{24} = -m_5\eta$
$A_{13} = m_5\left(\frac{\eta}{\zeta}\right)$	$A_{45} = (m_4+m_5)R_0 + m_5[\xi + \eta(\varphi_3-\varphi_2)]$	$A_{31} = m_5\left(\frac{\eta}{\zeta}\right)$	$A_{26} = m_5\left(1-\frac{2R_0\xi}{H_0\zeta}\right)$
$A_{14} = m_5(R_0+\xi)$	$A_{27} = -m_5\left[x_3(\varphi_3-\varphi_2) + y_3\right]$	$A_{33} = m_4+m_5$	$A_{25} = -m_5(\varphi_3-\varphi_2)$
$A_{62} = m_5\left(1-\frac{2R_0\xi}{H_0\zeta}\right)$	$A_{44} = (m_4+m_5)R_0^2 + m_5(2R_0\xi+\eta^2+\xi^2)$	$A_{32} = m_5\left(\frac{\xi}{\zeta}\right)$	$A_{41} = m_5(R_0+\xi)$
$A_{15} = m_5$	$A_{17} = m_5\left[x_3 + y_3(\varphi_3-\varphi_2)\right]$	$A_{51} = m_5$	$A_{52} = -m_5(\varphi_3-\varphi_2)$
$A_{610} = m_6\frac{2P_0}{H_0}$	$A_{54} = (m_4+m_5)R_0 + m_5[\xi + \eta(\varphi_3-\varphi_2)]$	$A_{57} = (m_3+m_4+m_5+m_6)x_3$	$A_{55} = m_3+m_4+m_5+m_6$
$A_{106} = m_6\frac{2P_0}{H_0}$	$A_{61} = -m_5\left((\varphi_3-\varphi_2) + \frac{2R_0\eta}{H_0\zeta}\right)$	$A_{67} = -(m_3+m_4+m_5+m_6)y_3$	$A_{63} = -(m_4+m_5)\frac{2R_0}{H_0}$
$A_{66} = m_3+m_4+m_5+m_6+(m_4+m_5)\frac{4R_0^2}{H_0^2} + m_6\frac{4P_0^2}{H_0^2}$		$A_{72} = -m_5\cdot\left[x_3(\varphi_3-\varphi_2) + y_3\right]$	$A_{71} = m_5\left[x_3 + y_3(\varphi_3-\varphi_2)\right]$
$A_{46} = -(m_4+m_5)R_0(\varphi_3-\varphi_2) - m_5[\xi(\varphi_3-\varphi_2)+\eta]$		$A_{59} = -m_6P_0$	$A_{69} = m_6P_0(\varphi_4-\varphi_2)$
$A_{46} = -(m_4+m_5)R_0(\varphi_3-\varphi_2) - m_5[\xi(\varphi_3-\varphi_2)+\eta]$		$A_{42} = -m_5\eta$	$A_{69} = m_6P_0(\varphi_4-\varphi_2)$
$A_{47} = (m_4+m_5)R_0[x_3 + y_3(\varphi_3-\varphi_2)] + m_5[x_3\xi + y_3\eta + (x_3\eta + y_3\xi)(\varphi_3-\varphi_2)]$			$A_{88} = J_1$
$A_{74} = (m_4+m_5)R_0[x_3 + y_3(\varphi_3-\varphi_2)] + m_5\left[(x_3\eta + y_3\xi)(\varphi_3-\varphi_2) + (y_3\eta + x_3\xi)\right]$			$A_{95} = -m_6P_0$
$A_{75} = (m_3+m_4+m_5+m_6)x_3$	$A_{79} = -m_6P_0[y_3(\varphi_4-\varphi_2) + x_3]$	$A_{71} = m_5\left[x_3 + y_3(\varphi_3-\varphi_2)\right]$	
$A_{76} = -(m_3+m_4+m_5+m_6)y_3$	$A_{97} = -m_6P_0\left[x_3 + y_3(\varphi_4-\varphi_2)\right]$	$A_{96} = m_6P_0(\varphi_4-\varphi_2)$	
$A_{77} = J_2 + (m_3+m_4+m_5+m_6)(x_3^2+y_3^2)$		$A_{99} = m_6P_0^2$	$A_{1010} = m_6$